Improved Mechanical and Thermomechanical Properties of Alumina Substrate via Iron Doping

Riko I Made*[1], Eric Jian Rong Phua[1,2], Stevin Snellius Pramana[1,3], Chee Cheong Wong[1], Zhong Chen[1], Alfred Iing Yoong Tok[1], Chee Lip Gan**[1],

*imaderiko@ntu.edu.sg

** clgan@ntu.edu.sg

[1]School of Materials Science and Engineering, Nanyang Technological University, Singapore. 50 Nanyang Avenue, Singapore 639798

[2]Institute of Microelectronics, Agency for Science, Technology and Research (A*STAR), 11 Science Park Road, Singapore Science Park II, Singapore 117685

[3]Facility for Analysis, Characterization, Testing and Simulation, Nanyang Technological University, 50 Nanyang Avenue, Singapore 639798

Abstracts

We present a method to improve the overall properties of sintered alumina substrate via iron doping that has a higher fracture toughness, lower thermal conductivity, lower thermal expansion coefficient and comparable dielectric constant to pure alumina. Such properties are beneficial for harsh environment electronic packages. X-Ray and electron probe micros analysis concluded that toughening are likely contributed by multiple phases strengthening and ruled out crack bridging or grain boundary strengthening.

Keywords: Ceramics, High temperature, harsh environment, Electronics packaging, High pressure.

Harsh environment applications typically use low power devices that do not generate much heat to be dissipated to the environment. On the contrary, it is necessary to prevent heat transfer from the environment to the device chip. For this purpose, low thermal conductivity substrate would be more suitable.

In this study, Al_2O_3 is selected mainly due to its low thermal conductivity, suitable electrical conducting properties, chemically stable at high temperature and is a particularly mature technology and inexpensive to produce or acquire. However, it has relatively high dielectric constant and high coefficient of thermal expansion (CTE) as compared to Si that may impose some reliability concerns.

Iron has been identified as a possible dopant for alumina substrates for such an application. Fe doping has been reported to decrease the transformation temperature of amorphous alumina η phase to crystalline α alumina [1], possibly improve alumina - metal adhesion [2] improve the alumina's fracture toughness by means of crack bridging mechanism due to the presence of ductile iron phase [1,3–5]. However, the presence of ductile iron phase may compromise the substrates electrical insulating properties. On the other hand, having fully oxidized Fe may not lead to strengthening by crack bridging mechanism nor that it will deteriorate the alumina's mechanical properties. In this work, we present systematical characterizations of the iron doped alumina substrate produced by powder methods.

A mixture of alumina with 10wt.% iron (Fe) was prepared by wet ball milling in alumina jar for 24 hours with 20:1 of ball to powder weight ratio. The resulting powder was uniaxially pressed to form pellets, followed by 200 MPa cold isostatic pressing. The resulting pellets were air sintered at 1500^{o}C for 12 hours.

Fracture toughness of the sample was deduced from the crack length measurement from Vickers indentation based on the following relation [6]

$$K_c = \xi_v^R \left(E/H\right)^{1/2} \left(P/c_o^{3/2}\right) \quad (1)$$

where P is the indentation peak load, c_o is the crack length, ξ_v^R = 0.016±0.004 is a material-independent constant for Vickers produced radial cracks [6], E is the Young's modulus and H is the materials hardness defined as

$$H = P/a_o\, a^2 \quad (2)$$

where a is the half diagonal of indentation length and $a_o = 2$ is a numerical constant for Vickers indenter. Sintered samples were indented with Vicker's pyramid shaped tip micro-indenter with 10 kgf load setting for 10 s dwell time. Commercially purchased sintered alumina samples from Xellatech Pte. Ltd. were also measured and used as a reference.

Thermal conductivity of sintered sample was deduced from the thermal diffusivity measurement by laser flash method. Thermal diffusivity was indirectly measured by observing the temperature changes on the front side of the sample by laser illumination from the back of the sample. Thus, the thermal conductivity was obtained by the following relation [7]

$$k = \alpha \rho C \quad (3)$$

where α is the thermal diffusivity, ρ is the density and C is the specific heat of the specimen.

Thermal expansion coefficient was deduced from measured linear dimensions change with respect to increasing heating (5°C/min) from 20°C to 400°C. Dielectric constant was obtained

from impedance measurement of sintered samples at 1 MHz frequency using Agilent 4284 A LCR-Meter.

Powder X-ray diffraction (XRD) using Bruker D8 Advance diffractometer with CuK_α radiation was used for phase analysis of ball milled and sintered samples. Rietveld refinements [8] were performed for phase quantification from XRD diffraction patterns. The weight percentage of each phase was calculated based on :

$$w_\alpha = \frac{S_\alpha (ZMV)_\alpha}{\sum_i S_i (ZMV)_i} \tag{4}$$

where w_α is the weight fraction of phase α, S is the Rietveld scale factor, Z is the number of formula units in unit cell, M is the molecular mass of the formula unit, V is the unit cell volume [9].

Field emission electron microscopy (FEI Nova 600i Nanolab) operating at 5 kV was used to observe the morphology of the samples. The samples were mirror-polished and carbon coated before the electron probe microanalysis (EPMA) was performed on JEOL JXA-8530F equipped with five wavelength dispersive spectrometers (WDS). The accelerating voltage and current used were 15 kV and 20 nA, respectively.

Comparisons of particle size between as purchased alumina, iron-powder and post ball milling of alumina with 10 wt.% Fe are given in Fig. 1(a) to (c), respectively. It can clearly be observed from secondary electron microscope imaging (SEI) that ball milling effectively reduces the particle size of the mixed powder.

It was found that Fe doped samples have a higher fracture toughness (6.12 ± 1.23 MPa/$m^{0.5}$) as compared to undoped reference samples (3.14 ± 0.88 MPa/$m^{0.5}$). The measured absolute density of the doped samples were higher (3.83 ± 0.02 g/cm^3) as compared to the reference sample (3.64 ± 0.22 g/cm^3), but both samples have similar relative mass density with respect to their theoretical mixture's density of 10 wt.% Fe (4.05 g/cm^3) and 0 wt.% Fe (4.00 g/cm^3) for doped and reference sample, respectively.

Doped samples also show a lower thermal diffusivity as compared to the reference sample, i.e. 5.11 ± 0.04 mm^2/s and 8.14 ± 0.09 mm^2/s, respectively. From differential scanning calorimetry (DSC) heating and cooling curves, both samples have heat capacity of ~ 0.765 J/gK at 25°C. Thus from eq. (3), we obtained that there is a reduction in thermal conductivity of doped samples from 22.43 ± 0.29 W/mK to 16.16 ± 1.91 W/mK.

Doped samples show CTE reduction from 8.40 ± 0.017 ppm/K to 6.91 ± 0.048 ppm/K. On the other hand, the relative dielectric constant is higher for the doped samples from the reference sample (10.36 ± 0.241 as compared to 9.9 ± 0.018).

X-ray diffraction (XRD) characterization of the as-prepared powder, reference and sintered samples are given in Fig. 2(a), (b) and (c), respectively. Rietveld refinement on the as-prepared powder shows that around 2.4 ± 0.1 wt % crystalline Fe remains in the form of Iron-metal, Hematite (Fe_2O_3) and Wüstite (FeO), from 10 wt% Fe initially added. Reduction in the detected quantity of Fe can be attributed to both the formation of amorphous Fe, and addition of alumina. The source of extra alumina could come from erosion debris of the ball milling's jar as well as the alumina ball during the ball milling process. Rietveld refinement also indicated that the

average grain-size from integrated breadth volume weighted mean column lengths [10] (LVol-IB) is 50 ± 8 nm.

On the other hand, the full width at half maximum observed from the XRD patterns of both the reference sample and sintered samples is narrower as compared to the as-prepared powder XRD pattern. The reference sample shows it consists mostly of alumina with an average grain-size (LVol-IB) of 128 ± 11 nm, with ~0.4 wt. % of MgO impurity, which is arguably beyond the XRD detection limit.

All *hkl* reflections can be identified as corundum Al_2O_3 phase with average crystallite size (LVol-IB) of 122 ± 10 nm, increase from 50 ± 8 nm from the unsintered powders. Neither crystalline Fe(bcc) nor other oxidized Fe was observed. The absence of Fe metal thus implies that fracture toughness increase is not contributed by crack bridging mechanism. Further refinement shows that ~2.5 wt % Fe (2.30 ± 0.04 at. %) has substituted for Al^{3+}. This substitution has expanded the unit cell, with their lattice parameter changed from a = 4.7591 Å and c = 12.9973 Å to $a = 4.7735 \pm 8.8\times10^{-4}$ Å and $c = 13.0293 \pm 3.8\times10^{-4}$ Å. No preferred orientation that may suggest abnormal grain growth was observed from the refinement. This result indicates that most of the available Fe has been oxidized to Fe^{3+} during sintering. The fact that Fe^{3+} is preferred than Fe^{2+} is due to Fe^{3+} ionic radius ($r_{Fe^{3+}}$ = 0.49 Å) is closer to the Al^{3+} ($r_{Al^{3+}}$ = 0.39 Å) as compared to the larger Fe^{2+} ($r_{Al^{3+}}$ = 0.63 Å)[11] and the oxygen site is fully occupied within the estimated standard deviation. The amorphization of the iron by ball milling was suspected to be negligible although further verifications still need to be conducted in the near future.

Backscattered electron (BSE) imaging coupled with electron probe micro analysis (EPMA) were used for compositional analysis. It reveals that the doped samples consist of three distinct phases as shown in Fig. 3 (a), labeled as α, β and γ, respectively. The first and the darkest phase α consists of around 99.49 ± 0.01 wt.% Alumina and 0.49 ± 0.01 wt.% Fe_2O_3. The second phase β with brighter appearance consists of 95.02 ± 0.18 wt.% Alumina and 4.95 ± 0.18 wt.% Fe_2O_3. Finally, the third phase γ appears the brightest, consists of 59.47 ± 0.76 wt.% Alumina, 20.99 ± 1.10 wt.% Fe_2O_3 and 19.54 ± 0.34 wt.% MgO. Grayscale image analysis on larger BSE scan (not shown) indicates that the β phase occupies ~90 % of the total area, followed by 8 % and 0.1 % of α and γ phase, respectively.

From the results, the reduction in thermal conductivity is as expected. Introducing Fe as dopants has effectively created defects to the alumina crystals, which increases phonon scattering probability, thus reducing the thermal conductivity.

The sources of difference in the CTE can be caused by porosity difference, matrix grain size differences or the presence of second phase. It is clear from the results that doped samples have a higher relative density as compared to the reference sample which may also indicate that there is less porosity in the doped sample. However, it has been reported that porosity does not affect CTE [12]. Furthermore, a higher mass density should lead to higher CTE as thermal motion of the particles have to be accommodated by thermal expansion [13].

Decrease in CTE has been reported in Mg/Al_2O_3 composite along with reduction in the grain size [14]. However, both doped and referenced samples are observed to have similar crystallite size

of 120 ± 10 nm and 128 ± 11 nm for doped and reference sample, respectively. Thus, contribution by grain size decrease to CTE reduction can be ruled out.

The presence of second phase is also reported to reduce the CTE [13,15,16]. Multiple phases are also reported to induce micro-cracking that provides the spaces necessary to accommodate particle thermal movement without thermal expansion [13]. As observed from EPMA shown in Fig. 3, the doped samples comprise of three phases. However, no micro-cracking was induced. Therefore, the CTE reduction may be attributed to the formation of second phase. It is not clear how the presence of second and third phases lead to a lower CTE as compositing effect of those three phases should have its CTE in between Al_2O_3 and Fe_2O_3, *i.e.* between 8.40 ± 0.017 and 9.9 ppm/K [17], respectively. Instead, sintered samples have CTE of 6.91 ± 0.048, which is lower than both Al_2O_3 and Fe_2O_3.

The small increase in dielectric constant could be caused by substitution of Fe^{3+} ion for Al^{3+} that induces local charge polarization [18]. By comparing their ionic radius, Fe^{3+} is larger than Al^{3+} [11], which indicates a stronger attraction of electron to Al [19]. This tendency may lead to the charge polarization on the doped samples; therefore doped samples have slightly higher dielectric constant.

It is well known that the presence of a second phase could improve ceramics fracture toughness [20]. Presence of a ductile phase, in this case Fe, could induce strengthening by means of crack bridging mechanism [4]. For this mechanism to work, it will require sufficient quantity of ductile phase of Fe-metal available after sintering. As mentioned earlier, XRD characterization of the sintered samples detected neither Fe(bcc) nor other unoxidized Fe. The absence of Fe thus implies that the increase in fracture toughness is not contributed by crack bridging mechanism.

Strengthening could also be contributed by grain size strengthening, whereby coarse grain have been reported to be less susceptible to fracture [21]. It is common to observe the increase in grain size as a result of heat treatment by mechanism of surface diffusion or bulk diffusion [22], which may lead to higher fracture toughness. Furthermore, increase in the grain size (and possibly inducing abnormal grain growth) might also be enhanced by Fe^{2+} diffusion assisted grain growth [3,23,24]

During sintering, Fe^{2+} that assist the sintering may become available from pre-existing FeO from the starting powder that lose their oxygen atoms or oxidation of Fe-metal that are available in the mixed powder. Meanwhile, Fe_2O_3 may not assist much to grain growth mechanism. However, the presence of Fe as a substitution for Al indicates that all Fe and Fe^{2+} were eventually oxidized to Fe^{3+}, which diminishes Fe^{2+} assisted grain growth [25]. Given the oxidation kinetics may be slow enough, Fe^{2+} may be present during sintering to induce the formation of oxygen vacancy to maintain the charge balance in the crystal, which leads to faster diffusion path and induces faster grain growth, thus induces larger grains after sintering [24]. However, the crystallite size of doped samples and reference sample are similar, which means that there was insufficient Fe^{2+} enhanced grain growth, hence grain size induced toughening was ruled out.

On the other hand, the toughening mechanism could be induced from the presence of non ductile phases as presented in Fig. 3, i.e. α, β and γ phases. The boundary between phases in some circumstances could act as crack arrest, thus increasing fracture toughness. Comparing BSE and XRD characterizations, it is understandable that γ phase was not detected by XRD scan due to their small quantity. However from EPMA characterizations, we can deduce that γ weight concentration corresponds to an atomic ratio of 1.78 : 0.4 : 0.74 : 4 for Al : Fe : Mg : O,

respectively. From there, we can roughly deduce that γ has the crystallochemical formula $[Mg_{0.74}Fe^{2+}_{0.22}\square_{0.04}][Al_{1.78}Fe^{3+}_{0.18}\square_{0.04}]O_4$, which can easily be magnesium aluminate spinel, with some Mg^{2+} substituted by Fe^{2+} and Al^{3+} by Fe^{3+} with the possible vacancies (□) at both sites. γ phase appearance has also been observed in co-doping of alumina with MgO and FeO [26]. By comparing Fe weight composition from both EPMA and XRD characterizations, we can deduce that there could be around ~0.98 wt % amorphous Fe phase, which can be arguably said that there is no amorphous Fe induced by ball milling within experimental error.

Assuming that quantity of amorphous Fe is negligible, the relative density of the doped sample need to be calculated based on 2.5 wt.% Fe, as deduced from XRD characterization stead of 10 wt.% Fe from initial mixture. The corrected relative density for the doped sample is 94.5 ± 0.06 %, which is higher than the reference sample.

The presence of MgO in the sintered samples is unexpected but understandable. Small quantity of MgO has been known to be used as alumina sintering additive to suppress the formation of alumina's abnormal grain growth, thus improving the final density [27]. From the EPMA results, we could also deduce that the diffraction pattern in XRD characterization was mostly due to β phase (as shown in Fig. 3 a), which occupies ~90 % of the scanned area. ~10 % composition by volume may be sufficient to induce crack arrest mechanism, and therefore increase the apparent fracture toughness.

In summary, we have seen that Fe doped alumina substrate could potentially be used for harsh environment electronic application. With comparable electrical properties, and potentially less CTE mismatch with silicon, usage of Fe doped alumina could lead to more reliable packaging solution. While the reduction in thermal conductivity can be attributed to an increase in phonon scattering, the reduction in CTE and the observed improvement in fracture toughness is most likely contributed by multiple phase strengthening.

The authors would also like to acknowledge SERC Grant No. 1021650081 for the support of this work. Authors also would like to acknowledge Dr S. Valavan from Republic Polytechnic Singapore for the access to thermal diffusivity measurement system.

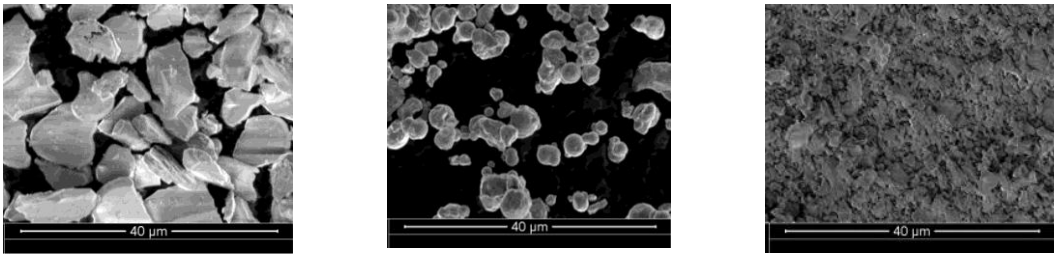

(a) **(b)** **(c)**

Fig. 1 Comparison of materials particle size. (a) Raw alumina powder, (b) iron powder, (c) ball milled mixture of alumina and iron powder.

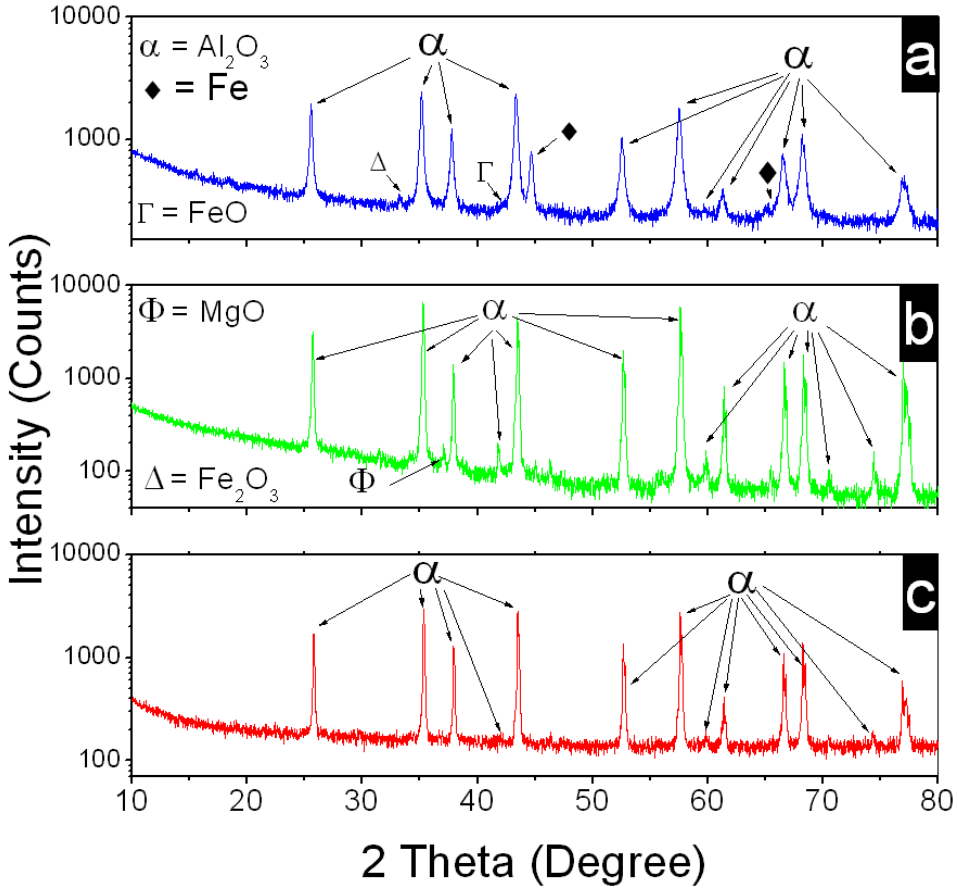

Fig. 2 X-Ray diffraction of ball milled powder, reference sample and sintered sample. (a) Ball milled powder, consists of mixture of Al_2O_3, FeO, and Fe_2O_3. After ball milling, only 2.4 ± 0.1 wt% Fe in the mixture, (b) reference sample with ~0.4 wt% MgO trace. (c) Sintered pellet, with 2.30 ± 0.04 at.% Fe in Fe^{3+} found to substitute Al^{3+}, equivalent to ~2.5 wt.% Fe.

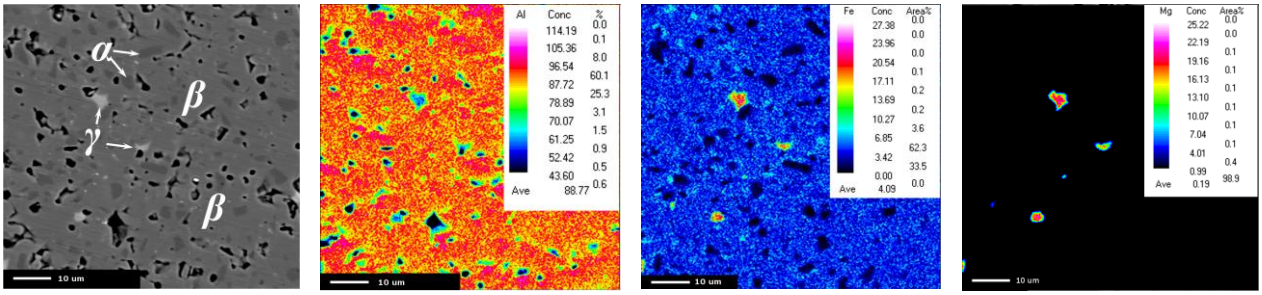

a b c d

Fig. 3 BSE-SEM coupled with EPMA elemental analysis. (a) Grey scale from BSE image showing three distinct phases, i.e. α , β and γ phase, (b) Aluminium map, (c) Fe map, (d) Mg map.

References

[1] X. Devaux, C. Laurent, A. Rousset, Nanostructured Materials 2 (1993) 339.
[2] R. Kondou, T. Suga, in:, Electronic Components and Technology Conference (ECTC), 2011 IEEE 61st, IEEE, Lake Buena Vista, FL, 2011, pp. 2165 –2170.
[3] P. Tartaj, J. Tartaj, Chem. Mater. 14 (2002) 536.
[4] P.A. Trusty, J.A. Yeomans, Journal of the European Ceramic Society 17 (1997) 495.
[5] J. Guichard, O. Tillement, A. Mocellin, Journal of Materials Science 32 (1997) 4513.
[6] G.R. Anstis, P. Chantikul, B.R. Lawn, D.B. Marshall, Journal of the American Ceramic Society 64 (1981) 533.
[7] F. Boey, A.I.Y. Tok, Y.C. Lam, S.Y. Chew, Materials Science and Engineering A 335 (2002) 281.
[8] H.M. Rietveld, Journal of Applied Crystallography 2 (1969) 65.
[9] R.J. Hill, C.J. Howard, Journal of Applied Crystallography 20 (1987) 467.
[10] A.R. Stokes, A.J.C. Wilson, Mathematical Proceedings of the Cambridge Philosophical Society 38 (1942) 313.
[11] R.D. Shannon, Acta Crystallographica Section A: Crystal Physics, Diffraction, Theoretical and General Crystallography 32 (1976) 751.
[12] R.L. Coble, W.D. Kingery, Journal of the American Ceramic Society 39 (1956) 377.
[13] P. Oikonomou, C. Dedeloudis, C.J. Stournaras, C. Ftikos, Journal of the European Ceramic Society 27 (2007) 3475.
[14] S.F. Hassan, M. Gupta, Composite Structures 72 (2006) 19.
[15] T. Hsieh, H. Choe, E.J. Lavernia, J. Wolfenstine, Materials Letters 30 (1997) 407.
[16] - , M. Jimenez-Melendo, A. - , G. Wötting, Journal of the European Ceramic Society 21 (2001) 63.
[17] S.B. Qadri, C. Fahed, H. Kim, A. Piqué, N.A. Mahadik, M.V. Rao, Physica Status Solidi (B) 248 (2011) 928.
[18] N. Ikeda, H. Ohsumi, K. Ohwada, K. Ishii, T. Inami, K. Kakurai, Y. Murakami, K. Yoshii, S. Mori, Y. Horibe, Nature 436 (2005) 1136.
[19] M. Birkholz, Zeitschrift Für Physik B Condensed Matter 96 (1995) 333.
[20] M. Farkash, D.. Brandon, Materials Science and Engineering: A 177 (1994) 269.
[21] S.-J. Cho, B.J. Hockey, B.R. Lawn, S.J. Bennison, Journal of the American Ceramic Society 72 (1989) 1249.
[22] R.L. Coble, Journal of the American Ceramic Society 41 (1958) 55.
[23] J. Tartaj, G.L. Messing, Journal of the European Ceramic Society 17 (1997) 719.
[24] W.R. Rao, I.B. Cutler, Journal of the American Ceramic Society 56 (1973) 588.
[25] R. Stößer, M. Nofz, M. Feist, G. Scholz, Journal of Solid State Chemistry 179 (2006) 652.
[26] J. Zhao, M.P. Harmer, Journal of the American Ceramic Society 70 (1987) 860.
[27] S.I. Bae, S. Baik, Journal of the American Ceramic Society 77 (1994) 2499.